



**HAL**  
open science

## Assessment of thermal change in cold avalanching glaciers in relation to climate warming

A. Gilbert, Christian Vincent, J. Krug, E. Berthier

### ► To cite this version:

A. Gilbert, Christian Vincent, J. Krug, E. Berthier. Assessment of thermal change in cold avalanching glaciers in relation to climate warming. *Geophysical Research Letters*, 2015, 42 (15), pp.6382-6390. 10.1002/2015GL064838 . insu-01217845

**HAL Id: insu-01217845**

**<https://insu.hal.science/insu-01217845>**

Submitted on 5 Mar 2021

**HAL** is a multi-disciplinary open access archive for the deposit and dissemination of scientific research documents, whether they are published or not. The documents may come from teaching and research institutions in France or abroad, or from public or private research centers.

L'archive ouverte pluridisciplinaire **HAL**, est destinée au dépôt et à la diffusion de documents scientifiques de niveau recherche, publiés ou non, émanant des établissements d'enseignement et de recherche français ou étrangers, des laboratoires publics ou privés.



## RESEARCH LETTER

10.1002/2015GL064838

## Key Points:

- Cold hanging glaciers below 3800 m in the Alps are becoming temperate
- Ice masses on steep slopes could become unstable during the current century in the Alps
- The risk related to hanging glaciers is going to considerably increase

## Supporting Information:

- Supporting Information S1

## Correspondence to:

A. Gilbert,  
adrieng@sfu.ca

## Citation:

Gilbert, A., C. Vincent, O. Gagliardini, J. Krug, and E. Berthier (2015), Assessment of thermal change in cold avalanching glaciers in relation to climate warming, *Geophys. Res. Lett.*, *42*, 6382–6390, doi:10.1002/2015GL064838.

Received 15 JUN 2015

Accepted 20 JUL 2015

Accepted article online 21 JUL 2015

Published online 6 AUG 2015

## Assessment of thermal change in cold avalanching glaciers in relation to climate warming

A. Gilbert<sup>1,2,3</sup>, C. Vincent<sup>1,2</sup>, O. Gagliardini<sup>1,2,4</sup>, J. Krug<sup>1,2</sup>, and E. Berthier<sup>5</sup>

<sup>1</sup>CNRS, LGGE (UMR5183), Grenoble, France, <sup>2</sup>Université Grenoble Alpes, LGGE (UMR5183), Grenoble, France, <sup>3</sup>Department of Earth Sciences, Simon Fraser University, Burnaby, British Columbia, Canada, <sup>4</sup>Institut Universitaire de France, Paris, France, <sup>5</sup>CNRS, Université de Toulouse, LEGOS, Toulouse, France

**Abstract** High-elevation glaciers covered by cold firn are undergoing substantial warming in response to ongoing climate change. This warming is affecting the ice/rock interface temperature, the primary driver of avalanching glacier instability on steep slopes. Prediction of future potential instability therefore requires appropriate modeling of the thermal evolution of these glaciers. Application of a state-of-the-art model to a glacier in the French Alps (Taconnaz) has provided the first evaluation of the temperature evolution of a cold hanging glacier through this century. Our observations and three-dimensional modeling of the glacier response (velocity, thickness, temperature, density, and water content) to climate change indicate that Taconnaz glacier will become temperate and potentially unstable over a large area by the end of the 21st century. The risk induced by this glacier hazard is high for the populated region below and makes observation and modeling of such glaciers a priority.

### 1. Introduction

The impact of climate change on avalanching glacier instabilities is difficult to assess [Haeberli *et al.*, 1997; Pralong and Funk, 2006; Faillettaz *et al.*, 2015]. However, such instabilities can lead to major disasters [Lliboutry, 1975; Evans *et al.*, 2009; Du Pasquier, 1896]. The stability of steep glaciers decreases when the basal temperature (at the interface between the ice and bedrock) reaches the pressure melting point [Alean, 1985; Huggel, 2008; Faillettaz *et al.*, 2011], creating conditions under which the glacier can slide on the rock [Cuffey and Paterson, 2010]. Modeling how cold glaciers will warm in the future in response to climatic change is therefore crucial. These glaciers are generally located at high elevations, above the equilibrium line, and the presence of cold firn makes them very sensitive (from a thermal point of view) to climate warming due to the possibility of surface meltwater percolation and refreezing [Suter, 2002; Gilbert *et al.*, 2014a]. Evidences show that cold glaciers at high elevations are warming [Vincent *et al.*, 2007a; Gilbert *et al.*, 2010; Hoelzle *et al.*, 2011] and a large number of cold hanging glaciers could become temperate before the end of the century. Quantifying this warming as a function of glacier characteristics and local climate change is therefore essential. Investigation of the thermal response of these glaciers requires a numerical modeling approach. However, this is challenging due to the generally complex geometry of hanging glaciers, the influence of firn on the rheology, the influence of ice advection on the temperature field, the importance of meltwater percolation and refreezing, and the intensity of strain heating.

The aim of this study is to provide a numerical modeling framework that can be used to assess the spatial and temporal evolution of the basal ice temperature and consequently the volume of ice that can become unstable in the future. Results from this numerical model should assist public authorities in assessing the hazards related to hanging glaciers that potentially threaten densely populated valleys. Because each glacier requires the development of a specially adapted model to take into account the features of its mass balance regime, bed topography, and elevation, it is virtually impossible to provide universal results concerning the destabilization of glaciers. Here we focus on Taconnaz glacier (Mont Blanc area, France), which is of particular interest in terms of hazard and offers a sufficient number of observations to constrain and validate the model. We present a fully coupled 3-D thermomechanical model applied to the upper part of the glacier (between 3300 and 4300 m above sea level (asl)) which is mostly cold and located on a steep slope (20 to 40°) above a 600 m wide and 60 to 100 m high ice cliff (see Figure 1). Many structures in the valley below are directly threatened by seracs falling from this hanging glacier [Naaim *et al.*, 2010]. Our study

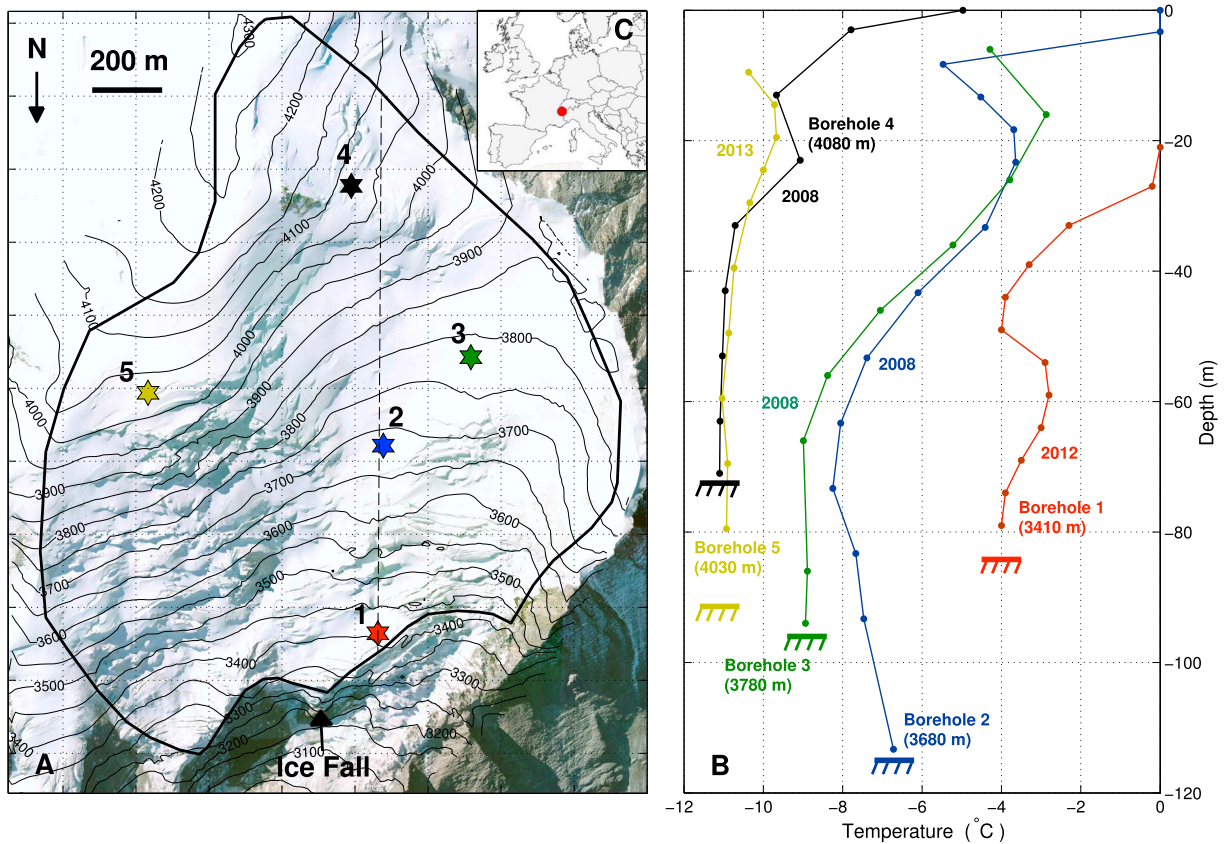


**Figure 1.** (a) Map of Taconnaz glacier. Colored stars show the locations of borehole temperature measurements, and the black bold line is the 3-D model domain. Elevation contours are shown for 50 m intervals. (b) Temperature profiles measured at the five boreholes at different dates. (c) Location of Taconnaz glacier (red dot).

provides the first evaluation of the temporal and spatial thermal response of an avalanching glacier to ongoing climate change.

### 2. Three-Dimensional Thermomechanical Model

The thermomechanical model used in this study has been presented in detail in *Gilbert et al.* [2014b]. This model was developed to simulate the thermal and mechanical response to climate change of the accumulation zone of polythermal glaciers. This model includes a full-Stokes flow model taking into account the firn rheology coupled with upper free-surface evolution, density evolution, enthalpy transport, meltwater percolation and refreezing, and a bedrock thermal model (see Table 1). The present study is the first application of the model to a complex three-dimensional case that includes strong advective processes. In order to take into account the mechanical degradation of the ice by intense crevassing, damage mechanics have been included in the model.

Firn and ice are considered to be one unique material with variable density; all the following equations are applied to whole glacier without distinction between firn and ice. The velocities are obtained by solving the momentum and mass conservation equations:

$$\text{div}(\sigma) + \rho g = 0 \tag{1}$$

$$\frac{\partial \rho}{\partial t} + \nabla \cdot (\rho \mathbf{v}) = \frac{Q_{\text{lat}}}{L} \tag{2}$$

where  $\sigma$  is the stress tensor (Pa),  $g$  acceleration due to gravity ( $\text{m s}^{-2}$ ),  $\rho$  the firn density,  $\mathbf{v}$  the velocity field ( $\text{m s}^{-1}$ ),  $Q_{\text{lat}}$  the latent heat released by meltwater refreezing (see equation (3)), and  $L$  the latent heat of fusion ( $\text{J kg}^{-1}$ ). The model includes a flow law for compressible firn as initially proposed by

**Table 1.** List of Variables Used in the Model

Variable Name	Symbol	Unit
Enthalpy	$H$	$\text{J kg}^{-1}$
Temperature	$T$	K
Water content	$\omega$	$\text{kg m}^{-3}$
Velocity	$\mathbf{v}$	$\text{m s}^{-1}$
Pressure	$P$	Pa
Density	$\rho$	$\text{kg m}^{-3}$
Surface elevation	$s$	m
Damage	$D$	-

*Gagliardini and Meyssonier* [1997]. This rheological law takes the form of Glen's flow law but accounts for compressibility by imposing a density-dependent relationship between stress and strain.

Energy transport is modeled using the enthalpy formulation proposed by *Aschwanden et al.* [2012]:

$$\rho \left( \frac{\partial H}{\partial t} + \mathbf{v} \cdot \nabla \mathbf{H} \right) = \nabla(\kappa \nabla \mathbf{H}) + \text{tr}(\sigma \dot{\epsilon}) + Q_{\text{lat}} \quad (3)$$

where  $H$  is the enthalpy ( $\text{J kg}^{-1}$ ),  $\kappa$  the enthalpy diffusivity ( $\text{kg m}^{-1} \text{s}^{-1}$ ),  $\text{tr}(\sigma \dot{\epsilon})$  the strain heating ( $\text{J m}^{-3} \text{s}^{-1}$ ), and  $Q_{\text{lat}}$  ( $\text{J m}^{-3} \text{s}^{-1}$ ) a source term accounting for meltwater refreezing.

Water percolation and refreezing is explicitly resolved assuming vertical water transport at constant velocity in order to calculate  $Q_{\text{lat}}$ . When the liquid water reaches the depth of pore closure density at  $830 \text{ kg m}^{-3}$  [*Cuffey and Paterson*, 2010], it is assumed to be evacuated by runoff along the firn/ice interface.

Glacier thickness evolution is computed by solving the free-surface equation:

$$\frac{\partial s}{\partial t} + u_s \frac{\partial s}{\partial x} + v_s \frac{\partial s}{\partial y} - w_s = \frac{\rho_w}{\rho_s} a_c \quad (4)$$

where  $s(x, y, t)$  is the free-surface elevation (m);  $u_s$ ,  $v_s$ , and  $w_s$  are the surface velocity components ( $\text{m s}^{-1}$ ) along the  $x$ ,  $y$ , and  $z$  axes, respectively;  $a_c$  is the surface mass balance (m water equivalent (w.e.)  $\text{s}^{-1}$ ),  $\rho_w$  the water density ( $\text{kg m}^{-3}$ ), and  $\rho_s$  the snow density at the surface ( $\text{kg m}^{-3}$ ).

Damage mechanics was included in the model following the approach of *Pralong and Funk* [2005] and *Krug et al.* [2014]. Considering the damage to be isotropic, it can be assumed that damage is a scalar quantity denoted  $D$  and the effective stress tensor can be written as follows:

$$\tilde{\sigma} = \frac{\sigma}{1 - D} \quad (5)$$

where  $\tilde{\sigma}$  is the effective Cauchy stress tensor and  $\sigma$  the Cauchy stress tensor. Damage evolution is computed using the following advection equation:

$$\frac{\partial D}{\partial t} + \mathbf{v} \cdot \nabla \mathbf{D} = \begin{cases} f(B, \chi) & \text{if } f(B, \chi) > 0 \\ 0 & \text{otherwise} \end{cases} \quad (6)$$

where the right-hand side represents a damage source term. This term is function of the damage enhancement factor  $B$  and the damage criterion  $\chi$ . As proposed by *Krug et al.* [2014], this criterion is expressed as a function of the maximum principal Cauchy stress  $\sigma_I$ , an average stress threshold for damage initiation  $\sigma_{\text{th}}$  and  $D$ :

$$\chi(\sigma_I, \sigma_{\text{th}}, D) = \max \left\{ 0, \frac{\sigma_I}{1 - D} - \sigma_{\text{th}} \right\} \quad (7)$$

The values of  $B$  and  $\sigma_{\text{th}}$  are set to  $1.0 \text{ MPa}^{-1}$  and  $0.03 \text{ MPa}$ , respectively [*Pralong and Funk*, 2005]. This is also in good agreement with *Krug et al.* [2014] who used these values with success for modeling calving on Helheim Glacier. The effective Cauchy stress tensor is then used instead of the Cauchy stress tensor in the flow law, which is equivalent in multiplying the flow rate factor by  $(1-D)^{-n}$ , where  $n$  is the Glen's law exponent.

### 3. Application to Taconnaz Glacier

#### 3.1. Observations

Numerous field campaigns have been carried out since the beginning of the 21st century to measure the surface velocity field, the surface mass balance [*Le Meur and Vincent*, 2006], the volume and frequency of serac falls [*Vincent et al.*, 2014], the bedrock and surface topography, and englacial temperatures. Bedrock

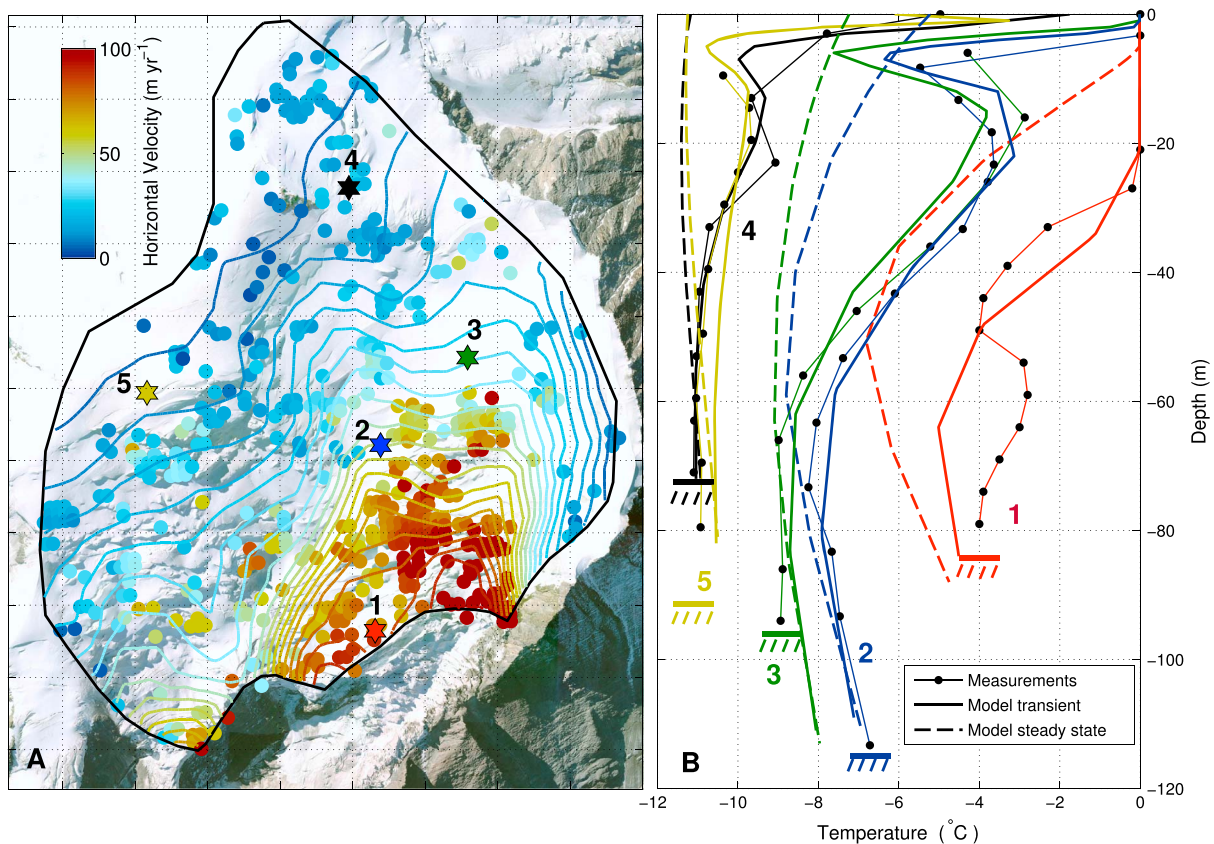


**Figure 2.** (a) Satellite-derived (colored dots) and modeled (colored contour lines) horizontal surface velocities. (b) Modeled steady state temperature profiles (bold dashed lines) and modeled transient profiles (bold solid lines) compared to the measurements at five drilling sites (thin lines with black dots).

topography was measured by a helicopter-borne radar survey in April 2011 using a frequency ranging from 50 to 100 MHz. A set of 55 profiles were obtained on the glacier at mean intervals of 50 m. Comparisons between inferred ice thickness from radar and drilling show a mean discrepancy of about 20 m (see Figure S5 in the supporting information). Surface topography was measured in August 2011 by airborne lidar (uncertainty less than 0.5 m). Temperatures profiles were measured in five different boreholes (Figure 1) by thermistor chains installed after hot water drilling between 2008 and 2013. Uncertainty is expected to be less than 0.1 K. The measurements for the different sites and years are plotted in Figure 1. They reveal that the glacier is mostly cold, with temperatures ranging from  $-11^{\circ}\text{C}$  to  $-4^{\circ}\text{C}$  at the glacier base. However, we observed the presence of temperate firn in the first 20 m at drilling site 1, indicating temperate surface conditions at this elevation (3400 m asl) even though the mean annual air temperature is about  $-4^{\circ}\text{C}$ . Surface velocities between 23 August and 19 September 2003 were measured using feature tracking applied to two 2.5 m SPOT5 satellite images [Berthier *et al.*, 2005]. After discarding unrealistic velocities, measurements were obtained for 537 points on Tacconnaz glacier and range from less than  $10\text{ m yr}^{-1}$  at the Dome du Gouter summit up to  $100\text{ m yr}^{-1}$  close to the ice fall (Figure 2). Their accuracy was estimated at about  $10\text{ m yr}^{-1}$  using D-GPS measurements on the Mer de Glace and Argentière Glacier [Berthier *et al.*, 2005]. This uncertainty is confirmed using D-GPS measurements available on Tacconnaz glacier (see supporting information Figure S3).

### 3.2. Model Setup

The mathematical model has been solved using the finite element code Elmer/Ice [e.g., Gagliardini *et al.*, 2013] based on the Elmer open-source multiphysics package (see <http://elmerice.elmerfem.org>). Details on the three-dimensional mesh and on the different boundary conditions are given in the supporting information (Text S1 and Figure S1 in the supporting information).

### 3.2.1. Steady State Simulation

In order to determine initial conditions at the beginning of the twentieth century for the transient simulations, a steady state configuration was modeled for the glacier. We assume that the glacier thickness remained nearly unchanged over the last century as observed at Col du Dôme just above Taconnaz glacier [Vincent *et al.*, 2007b] and the current thickness is therefore considered to be representative of the glacier in steady state. This assumption is confirmed by the present modeling results that show very little change in thickness over the twentieth century (<5 m). Mean surface mass balance data were taken from *Le Meur and Vincent* [2006]. This mass balance reconstruction is, however, poorly constrain (sparse measurements) and need bias correction. We multiplied the reconstructed accumulation rate by a factor of 1.4 in order to match the observed glacier thickness. Surface temperatures for steady conditions were directly adjusted for elevation so that the simulated basal temperatures would agree with the measured temperatures at the bottom of the five boreholes (Figure 2). For the numerical experiments, we assume a basal heat flux of  $1.5 \times 10^{-2} \text{ W m}^{-2}$  [Gilbert *et al.*, 2014b]. Exposed rock temperature below the icefall is set to the mean annual air temperature at this elevation (according to Lyon-Bron air temperature records and a constant lapse rate, see next section). Firn surface density is assumed to be constant over the whole glacier and set to  $350 \text{ kg m}^{-3}$  [Gilbert *et al.*, 2014a]. Surface damage is also imposed as a Dirichlet boundary condition and set to zero.

### 3.2.2. Transient Simulation

Starting from the steady state glacier, transient simulations are performed at a daily time step to solve the enthalpy and water percolation equations. Other variables are solved with a 100 day time step. The time-dependent boundary conditions are limited to surface melting, temperature, and mass balance. We assume a nonsliding condition at the base of the glacier even when the glacier bed becomes temperate.

Surface temperature is calculated as a function of air temperature using a constant lapse rate [Gilbert *et al.*, 2014b]. We used daily air temperatures recorded at Lyon-Bron station (~200 km west of the glacier) from 1907 to 2013. This temperature data set has already been successfully used for modeling glacier thermal regime in the area [Gilbert *et al.*, 2014a, 2014b]. Future daily temperature scenarios used in this study come from the ENSEMBLES climate scenario database ([www.ensembles-eu.org](http://www.ensembles-eu.org)) [Van der Linden and Mitchell, 2009] from which we selected three models in order to have different temperature variability: CNRM-RM5.1\_ARPEGE, METNOHIRHAM\_HadCM3Q0, and MPI-M-REMO\_ECHAM5. Climate scenarios were produced by Regional Climate Models forced by Global Circulation Models using the A1B scenario [Nakicenovic *et al.*, 2000] and downscaled using the empirical-statistical error correction method (quantile mapping [Themessl *et al.*, 2011]) at Col du Grand Saint Bernard meteorological station located 50 km east of the glacier at 2469 m asl. The annual temperature trends for these scenarios were then adjusted according to three new Representative Concentration Pathway (RCP) scenarios (2.6, 6.0, and 8.5) from last Intergovernmental Panel on Climate Change report [Collins *et al.*, 2013] (see supporting information Figure S2). We thus obtained nine climate scenarios (three RCPs for each of three models). Hereafter, only the average of the three models for each RCP will be presented (Figures 3 and 4).

Surface melting is calculated using a degree-day formulation including potential solar radiation dependence and a daily maximum temperature anomaly [Gilbert *et al.*, 2014a]. We added a dependence on elevation to account for albedo increase with elevation [Vincent, 2002]. Melting factor and elevation lapse rate were adjusted in order to match the measured temperature profiles (Figure 2). The temperature lapse rate was set to  $6.2 \times 10^{-2} \text{ K m}^{-1}$  and the melt factor calculated from

$$m_f = 2.05 \cdot 10^{-3} - 6.33 \cdot 10^{-7} z_s + 5.0 \cdot 10^{-6} R \quad (8)$$

where  $m_f$  is the melt factor (m w. e.  $\text{K}^{-1} \text{ d}^{-1}$ ),  $z_s$  the surface elevation (m), and  $R$  the annual mean potential solar radiation ( $\text{W m}^{-2}$ ).

The surface mass balance is calculated from the surface melt (computed as described above) and a constant accumulation rate. This accumulation rate is defined as the difference between the steady mass balance (section 3.2.1) and the mean melting calculated over the first decades of the twentieth century for which the glacier mass balance was close to steady state conditions [Vincent, 2002].

## 3.3. Results

Modeling results are in good agreement with observed temperature, velocity, and glacier thickness (Figure 2 and supporting information Figures S4 and S5). Simulations performed over the twentieth century reveal that

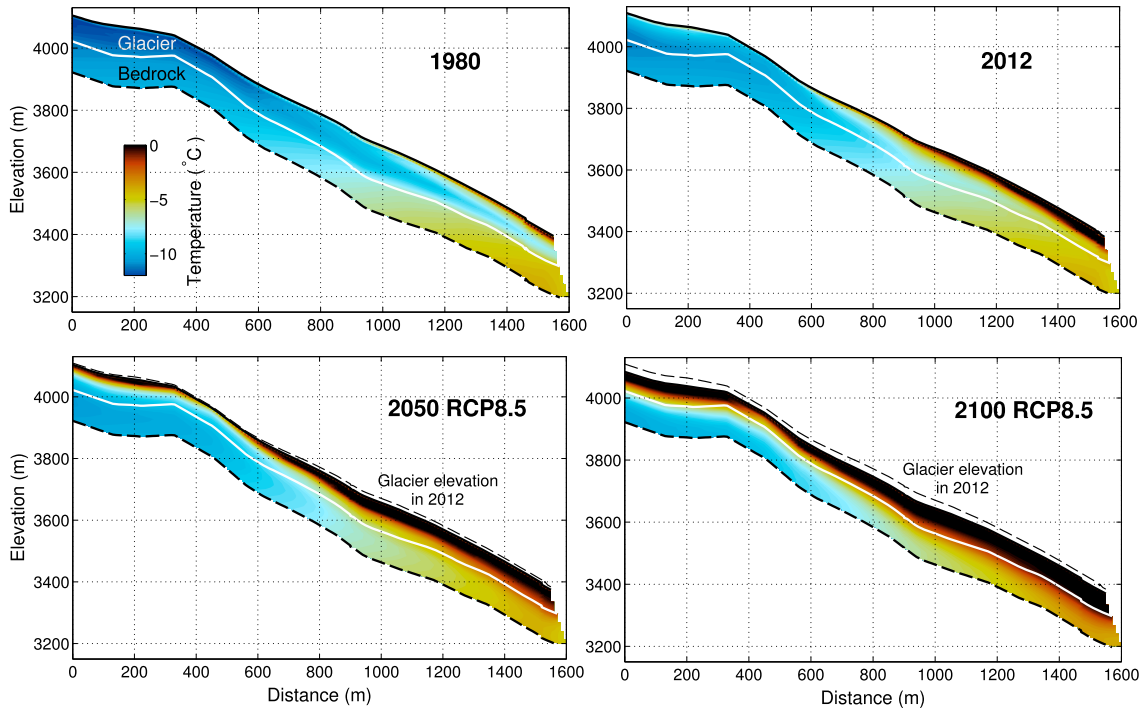


**Figure 3.** Modeled englacial temperatures along the longitudinal profile in Figure 1 (thin dashed line). The white line indicates the ice/rock transition. The thick dashed black line is the lower bedrock boundary in the model. The thin dashed black line is the 2012 surface elevation.

the glacier ice and its surface firn were mostly cold until 1980. After this time, a temperate firn layer started to develop in the lower part of the glacier above the icefall (Figure 3) in response to significant air temperature increasing (see supporting information Figure S2). This temperate layer reached a depth of 20 m in 2012 as observed and modeled at borehole 1 (Figure 2). The total volume of temperate firn/ice increased from about  $3.4 \times 10^6 \text{ m}^3$  (2% of the total glacier volume) at the beginning of twentieth century to about  $1.7 \times 10^7 \text{ m}^3$  (10% of the total volume) in 2012. The warm anomaly observed at around 60 m depth in borehole 1 is not captured by the model and reveals that the glacier could be locally influenced by

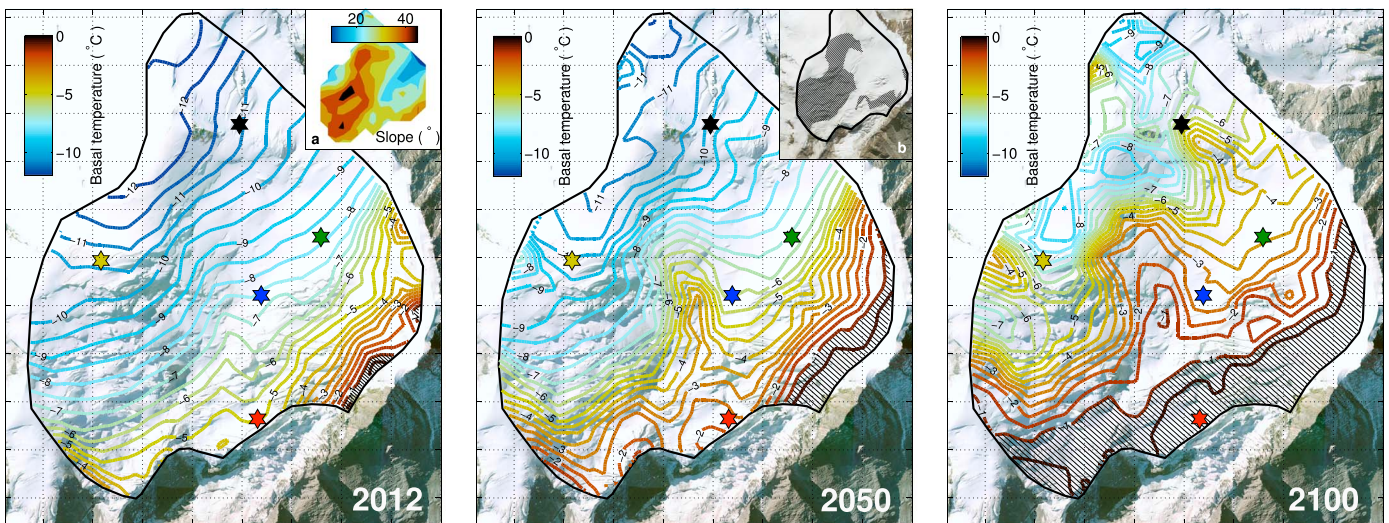


**Figure 4.** Modeled temperatures at the ice/rock interface for climate scenario RCP8.5. The areas over which temperature exceeds  $-1^\circ\text{C}$  are hatched. The inset a on the left plot shows the surface slope in degrees. The black hatched zone in inset b shows damage production location ( $f(B, \chi)$  in equation (6)).

crevasses that allow deeper water percolation and refreezing. However, due to high advection of cold ice from upstream, this kind of anomaly does not have the time to propagate very far and should not influence the general basal temperature pattern. The influence of damage mechanics is mainly expressed in the modeled thickness and velocity fields, because damage alters the flow rate factor by reducing ice viscosity. Surface velocity increase due to damage is about 10% in the most impacted zones. The maximum decrease in glacier thickness reaches 15 m upstream of borehole 2 (supporting information Figure S7).

Simulations for future climate conditions show that the temperate firn layer will extend to the highest elevation of the glacier (4300 m asl) before 2050 for all scenarios (Figure 3). Due to the efficiency of melting, percolation, and refreezing processes in transporting energy within the glacier [Gilbert *et al.*, 2014a], the firn warms very quickly, leading to a rapid increase of the temperate firn layer thickness. Below the firn/ice interface, the speed of propagation of the 0°C isotherm to bedrock is strongly limited by the impermeability of the cold ice to water. Energy transfer within the ice is limited to advective and diffusive processes, leading to slower warming rates. However, the extension of temperate ice down to the bedrock appears inevitable given that surface conditions will become temperate at all elevations. In the lower part of the glacier (above the icefall), ice at the bedrock interface should reach the melting point near 2080 and the temperate area will then progressively extend to higher elevations (Figures 3 and 4) for scenario RCP6.0 and RCP8.5 (see also supporting information Figures S11 to S14). The volume of temperate ice should reach  $7.0 \times 10^7 \text{ m}^3$  (40% of the total volume) in 2100 for RCP8.5 (supporting information Figure S15). The western region of the glacier should warm most quickly due to easterly aspect (enhancing surface melt) and the absence of cold ice in flow from upstream. The bedrock interface in this region of the glacier was already temperate over a small area in 2012 (Figure 4).

#### 4. Discussion and Conclusion

Three main processes have been identified that control the temperature field of a hanging glacier such as Tacconnaz: (i) the surface melting driven by elevation as well as surface slope and aspect, (ii) ice advection, and (iii) strain heating. In terms of temporal and spatial variability, surface melting appears to be a key parameter for this type of cold firn-covered glacier. It makes near-surface firn temperature highly sensitive to slope, aspect, elevation, and climate variation. Surface melting must be carefully taken into account for englacial temperature modeling of this kind. Numerical experiments show that cold ice advection is able to maintain cold basal conditions in the vicinity of the ice fall, despite temperate surface conditions and strain heating sufficient to increase basal temperature by several degrees (3 to 5 K close to the ice fall, see supporting information Figure S8). We show that the basal temperature increase due to strain heating is linearly correlated with the magnitude of surface ice flow velocities ( $R^2 = 0.92$ ) and is far from negligible in such no-sliding steep glaciers (see supporting information Figure S9). The thermal impact of the exposed rock downstream of the ice fall on the basal ice temperature is extremely low due to the inefficiency of heat diffusion compared to ice advection. Our numerical experiments show that the influence of exposed rock on basal ice temperature is limited to the first 15–20 m from the ice fall and the induced cooling is less than 1 K (see supporting information Figure S8).

For the assessment of potential hazards related to this glacier, our study offers two main results. First, the glacier thinning in response to mass balance and viscosity changes will not exceed 20 m in the vicinity of the ice fall by 2100. Second, our numerical experiments show that temperate ice will extend nearly to bedrock over a large area (Figure 4); it is therefore very likely that a large volume of ice could become temperate at its base in this century. Instabilities due to the transition from cold to temperate bed conditions have already been observed in the Alps with the catastrophic breakoff of Altels Glacier in 1895 [Heim, 1895; Forel, 1895; Du Pasquier, 1896]. The ice volume released was estimated at  $4 \times 10^6 \text{ m}^3$ , making this the largest known icefall event in the Alps. This glacier, located on a steep slope (35° to 40°), most likely experienced a rapid warming leading to a weakening of the basal support [Faillettaz *et al.*, 2011]. For the sake of comparison, the modeled volume of warm-based ice in 2100 located on a slope greater than 30° (see Figure 4) in Tacconnaz glacier would be about  $10 \times 10^6 \text{ m}^3$ . However, in the case of Altels breakoff event, bedrock temperature configuration was different with a cold glacier bed at the front and a temperate bed in the middle of the glacier creating meltwater entrapment that was likely responsible for the breakoff [Faillettaz *et al.*, 2011]. In our case, according to the different simulations, the onset of the

temperate ice/bedrock interface will initiate at the terminus (near ice cliff), independently of the climatic scenario. As a consequence, subglacial meltwater would not be trapped within the glacier as meltwater reaching the bed would have the possibility to be evacuated as runoff. In this case, the glacier is more likely to fail progressively in the release of small/medium ice chunks as the temperate zone extends upward. However, one of the main limitations of our model is that we do not take into account the fact that meltwater could reach the bed even in cold ice via crevasses. Crevasses would most likely be localized in the damage production zone in the middle of the east side of the glacier (see localization of the damage production in Figure 4, inset b). Similar to Altels glacier, this process could therefore create a temperate zone in the middle of the glacier, especially if the water supply increases with surface melt as the climate warms. Another limitation of our study is that we neglect the influence of sliding when the glacier bed becomes temperate. Sliding strongly influences the dynamics and possibly the thermal regime of the glacier. It is furthermore a central issue for studying glacier stability. Including a sliding law should be the next step toward a real estimation of glacier stability.

Modeling and measuring the progressive warming of cold hanging glaciers is a necessarily step to assess their stability [Faillettaz *et al.*, 2015]. This study presents the first model capable of reproducing most of the observed geometric and thermal characteristics of such a glacier, including the spatial and temporal evolution of the glacier bed temperature. Many cold glaciers in the Alps are located at elevations similar to those of Taconnaz glacier and are subject to similar warming. Given the climate projections, steep cold hanging glaciers located below 4000 m asl are likely to become partially temperate by the end of this century. Modeling and measuring the thermal evolution of such glaciers should be a priority for glacier hazard prediction.

#### Acknowledgments

This study was funded by the ACQWA (212250) and GLARISKALP European programs. It was also supported by the GLACIOCLIM observation network. We thank P. Possenti and L. Piard for conducting drilling operations and for their help in the field. We thank Météo-France for providing the meteorological data used in this study. The other data used in this study are available on request from Christian Vincent (christian.vincent@ujf-grenoble.fr). We thank H. Harder who revised the English of the manuscript.

The Editor thanks Jerome Faillettaz for his assistance in evaluating this paper.

#### References

- Alean, J. (1985), Ice avalanches: Some empirical information about their formation and reach, *J. Glaciol.*, *31*(109), 324–333.
- Aschwanden, A., E. Bueler, C. Khroulev, and H. Blatter (2012), An enthalpy formulation for glaciers and ice sheets, *J. Glaciol.*, *58*(209), 441–457.
- Berthier, E., H. Vardon, D. Baratoux, Y. Arnaud, C. Vincent, K. L. Feigl, F. Rémy, and B. Legrézy (2005), Surface motion of mountain glaciers derived from satellite optical imagery, *Remote Sens. Environ.*, *95*(1), 14–28.
- Collins, M., et al. (2013), Long-term climate change: Projections, commitments and irreversibility, in *Climate Change 2013: The Physical Science Basis. Contribution of Working Group I to the Fifth Assessment Report of the Intergovernmental Panel on Climate Change*, edited by T. F. Stocker et al., Cambridge Univ. Press, Cambridge, U. K., and New York.
- Cuffey, K., and W. B. S. Paterson (2010), *The Physics of Glaciers*, 4th ed., Academic Press, Amsterdam.
- Du Pasquier, L. (1896), L'avalanche du glacier de l'Altels le 11 septembre 1895, *Ann. Geophys.*, *5*(23), 458–468.
- Evans, S., O. Tutubalina, V. Drabyshev, S. Chernomorets, S. McDougall, D. Petrakov, and O. Hungr (2009), Catastrophic detachment and high-velocity long-run out flow of Kolka glacier, Caucasus mountains, Russia in 2002, *Geomorphology*, *105*, 314–321, doi:10.1016/j.geomorph.2008.10.008.
- Faillettaz, J., D. Sornette, and M. Funk (2011), Numerical modeling of a gravity-driven instability of a cold hanging glacier: Reanalysis of the 1895 break-off of Altelsgletscher, Switzerland, *J. Glaciol.*, *57*(205), 817–831.
- Faillettaz, J., M. Funk, and C. Vincent (2015), Avalanching glacier instabilities: Review on processes and early warning perspectives, *Rev. Geophys.*, *53*, 203–224, doi:10.1002/2014RG000466.
- Forel, F. A. (1895), *L'éboulement du Glacier de l'Altels*, *Archive des Sciences Physiques et Naturelles*, vol. 34, pp. 513–543, Genève.
- Gagliardini, O., and J. Meyssonier (1997), Flow simulation of a firm-covered cold glacier, *Ann. Glaciol.*, *24*, 242–248.
- Gagliardini, O., et al. (2013), Capabilities and performance of Elmer/Ice, a new-generation ice sheet model, *Geosci. Model Dev.*, *6*, 1299–1318, doi:10.5194/gmd-6-1299-2013.
- Gilbert, A., P. Wagnon, C. Vincent, P. Ginot, and M. Funk (2010), Atmospheric warming at a high elevation tropical site revealed by englacial temperatures at Illimani, Bolivia (6340 m above sea level, 16°S, 67°W), *J. Geophys. Res.*, *115*, D10109, doi:10.1029/2009JD012961.
- Gilbert, A., C. Vincent, D. Six, P. Wagnon, L. Piard, and P. Ginot (2014a), Modeling firn near-surface temperature in a cold accumulation zone (Col du Dôme, French Alps): From physical to semi-parameterized approach, *Cryosphere*, *8*, 689–703, doi:10.5194/tc-8-689-2014.
- Gilbert, A., O. Gagliardini, C. Vincent, and P. Wagnon (2014b), A 3-D thermal regime model suitable for cold accumulation zones of polythermal mountain glaciers, *J. Geophys. Res. Earth Surf.*, *119*, 1876–1893, doi:10.1002/2014JF003199.
- Haeberli, W., M. Wegmann, and D. Vonder Muehll (1997), Slope stability problems related to glacier shrinkage and permafrost degradation in the Alps, *Eclogae Geol. Helv.*, *90*, 407–414.
- Heim, A. (1895), *Die Gletscherlawine an der Altels am 11*, Zürcher und Furrer, Zürich.
- Hoelzle, M., G. Darms, M. P. Lüthi, and S. Suter (2011), Evidence of accelerated englacial warming in the Monte Rosa area Switzerland/Italy, *Cryosphere*, *5*, 231–243, doi:10.5194/tc-5-231-2011.
- Huggel, C. (2008), Recent extreme slope failures in glacial environments: Effects of thermal perturbation, *Quat. Sci. Rev.*, *28*(11–12), 1119–1130, doi:10.1016/j.quascirev.2008.06.007.
- Krug, J., J. Weiss, O. Gagliardini, and G. Durand (2014), Combining damage and fracture mechanics to model calving, *Cryosphere*, *8*, 2101–2117, doi:10.5194/tc-8-2101-2014.
- Le Meur, E., and C. Vincent (2006), Monitoring of the Taconnaz ice fall (French Alps) using measurements of mass balance, surface velocities and ice cliff position, *Cold Reg. Sci. Technol.*, *46*(1), 1–11.
- Llibouty, L. (1975), La catastrophe du Yungay (Perou), in *Proceedings of the Snow and Ice Symposium*, pp. 353–363, Moscow, August 1971.
- Naaim, M., T. Faug, F. Naaim, and N. Eckert (2010), Return period calculation and passive structure design at the Taconnaz avalanche path, France, *Ann. Glaciol.*, *51*(54), 89–97.

- Nakicenovic, N., et al. (2000), *IPCC Special Report on Emissions Scenarios*, Cambridge Univ. Press, Cambridge, U. K., and New York.
- Pralong, A., and M. Funk (2005), Dynamic damage model of crevasse opening and application to glacier calving, *J. Geophys. Res.*, *110*, B01309, doi:10.1029/2004JB003104.
- Pralong, A., and M. Funk (2006), On the instability of avalanching glaciers, *J. Glaciol.*, *52*(176), 31–48, doi:10.3189/172756506781828980.
- Suter, S. (2002), Cold firn and ice in the Monte Rosa and Mont Blanc areas: Spatial occurrence, surface energy balance and climatic evidence, PhD thesis, ETH Zürich.
- Themessl, M., A. Gobiet, and A. Leuprecht (2011), Empirical-statistical downscaling and error correction of daily precipitation from regional climate models, *Int. J. Climatol.*, *31*(10), 1530–1544.
- Van der Linden, P., and J. F. B. Mitchell (Eds.) (2009), *ENSEMBLES: Climate Change and Its Impacts: Summary of Research and Its Results From the ENSEMBLES Project*, Met Office Hadley Center, Exeter.
- Vincent, C. (2002), Influence of climate change over the 20th century on four French glacier mass balances, *J. Geophys. Res.*, *107*(D19), 4375, doi:10.1029/2001JD000832.
- Vincent, C., E. Le Meur, D. Six, P. Possenti, E. Lefebvre, and M. Funk (2007a), Climate warming revealed by englacial temperatures at Col du Dôme (4250 m, Mont-Blanc area), *Geophys. Res. Lett.*, *34*, L16502, doi:10.1029/2007GL029933.
- Vincent, C., E. Le Meur, D. Six, M. Funk, M. Hoelzle, and S. Preunkert (2007b), Very high-elevation Mont Blanc glaciated areas not affected by the 20th century climate change, *J. Geophys. Res.*, *112*, D09120, doi:10.1029/2006JD007407.
- Vincent, C., E. Thibert, M. Harter, A. Soruco, and A. Gilbert (2014), Volume and frequency of ice avalanches from the Tacconnaz hanging glacier (French Alps), *Ann. Glaciol.*, *56*(70), 17–25, doi:10.3189/2015AoG70A017.